

# Extension of Surface Roughness Model for Navier-Stokes Equation Based Aircraft Icing Code

Seungin Min\*, Chankyu Son\* and Kwanjung Yee\*  
Corresponding author: [kjyee@snu.ac.kr](mailto:kjyee@snu.ac.kr)

\* Seoul National University, Republic of Korea.

**Abstract:** Surface roughness should be taken into account when numerically predicting the aircraft icing shape since it affects the underlying physics of the frozen surface. Empirical correlation equation which introduces the uniform value of roughness based on experimental results has been widely used due to its simplicity and limitations of numerical methods for applying the physical model. Through this paper, the physical roughness models that present the roughness height varying depending on the state of the surface is introduced. Also, the differences between each model are compared, and the physical roughness model applicable to RANS based aircraft icing code is proposed. When applying the model, the analytical solution for the film and bead height is derived based on the modified governing equation. Then, through the force equilibrium equation, surface roughness and surface state are determined by comparing the external force and surface tension force. For the validation of the model, the roughness height, heat convection coefficients and shapes were presented. The qualitative discussion is made for the change in shape, and the necessity of the model was presented compared with the result of empirical correlation.

*Keywords:* Aircraft icing, Surface roughness, Heat convection coefficient.

## 1 Introduction

When the aircraft operates in cold and humid environments, super-cooled droplets in the atmosphere collide with the aircraft surface, resulting in ice accretion. Components of the aircraft exposed to freezing cause problem such as malfunction or performance deterioration, which poses a serious threat to the aircraft operation safety. In order to avoid such a phenomenon, numerical simulations have been used to predict the shape deformation due to aircraft icing with the effective means of analyzing water impingement and heat transfer effects. However, the numerical simulations predicts the macroscopic shapes, while microscopic characteristics such as surface roughness are represented through numerical modeling. Previous studies have shown that numerically predicted ice shape varying with surface roughness height. Therefore, the numerical modeling of the surface roughness affects the accuracy of the aircraft icing code.

The main factors of aircraft icing are the solidification due to heat transfer and water flow rate on the surface. When a water droplet freezes, it changes the surface roughness, thereby affecting the thermal gradient, which is responsible for the convective heat transfer and eventually associated with the final ice formation. Hansmann[1] observed qualitative changes in surface roughness on iced surface through a high-speed camera. He demonstrated that the water droplets coagulated into bead, rivulet and film

affected by the gravity, surface tension and aerodynamic forces. Shin and Anderson[2, 3] quantitatively analyzed the surface roughness of the iced airfoil. The surface of the aircraft was divided into three stages: a smooth region, a rough region, and a feather region. Shin [2] measured the surface roughness and measured surface roughness of about 0.28 ~ 0.79 mm especially in the rough region formed at the initial stage of icing.

Though it is important to consider the surface roughness in aircraft icing, in the early numerical simulations, the surface roughness value used in the integral boundary layer equation was defined by the users to estimate the ice shape as in experiments [4]. Then, due to the absence of a quantitative correlation between the roughness elements, an empirical correlation based on the experimental results with respect to the velocity, temperature, and liquid water content (LWC) was adopted, which provided the linear relation for each parameter [5]. This empirical correlation is widely used because of the merit that it can determine the surface roughness height simply with the ambient condition. However, there is crude consideration of the physical phenomena appearing on the surface.

To present the physical changes of the surface, Fortin[6] proposed a physical model using analytical solutions. He classified the surface into bead, rivulet and water film and computed roughness height. The model predicted the change of heat transfer coefficient according to the surface roughness according to the boundary layer theory and improved the result of the 2-dimensional aircraft icing code based on the panel method.

Croce [7] simulated the change of surface roughness through numerical analysis as a preliminary study to apply surface roughness model to FENSAP-ICE [8], an icing code developed by McGill University. The surface roughness of a plate was calculated using the Lagrangian method by tracking motion of each droplet. However, applying this method to all of the droplets requires large computational resources. Therefore, the model was not applied to aircraft icing codes, but it has laid a heuristic approach for advanced modeling based on physical phenomena.

In this study, we applied the surface roughness model to the RANS(Reynolds-averaged Navier-Stokes) based Aircraft icing code by extending the physical models presented in the previous study. For this, the surface was divided into beads, rivulets, and water film as Fortin[6] suggested, and the roughness height was calculated through the force equilibrium equation acting on the surface. The effect of the model is presented by the convective heat transfer coefficient derived from the turbulence model. In order to show the validity of the model application, the parameters such as roughness height and heat convection coefficient was presented. Also final ice accretion shapes were compared with the result by NASA's empirical correlation model and experiment.

## 2 Methodology

The aircraft icing code, as shown in Fig. 1, consists of four modules. Each module sequentially computes the aerodynamic force, droplet trajectory, thermodynamics, and shape deformation. Though aircraft icing is an inherently unsteady phenomenon lasting from a few to tens of minutes, a quasi-steady state is assumed for computational efficiency. The aircraft icing code, as shown in Fig. 1, consists of four modules. Each module sequentially computes the aerodynamic force, droplet trajectory, thermodynamics, and shape deformation. Though aircraft icing is an inherently unsteady phenomenon lasting from a few to tens of minutes, a quasi-steady state is assumed for computational efficiency. To consider the impact of shape change due to icing, a multi-shot method that divides the total icing time into several steps to account for the ice accretion as a function of time is used. The model is built in OpenFOAM<sup>TM</sup> [9], an open source code.

The unsteady RANS equation was used for the aerodynamic calculation and the modified Spalart-Allmaras model [10] was applied for the turbulence model to show the surface roughness effect due to the icing phenomenon. Each module is validated and detailed description can be found in the work by Son et. al[11].

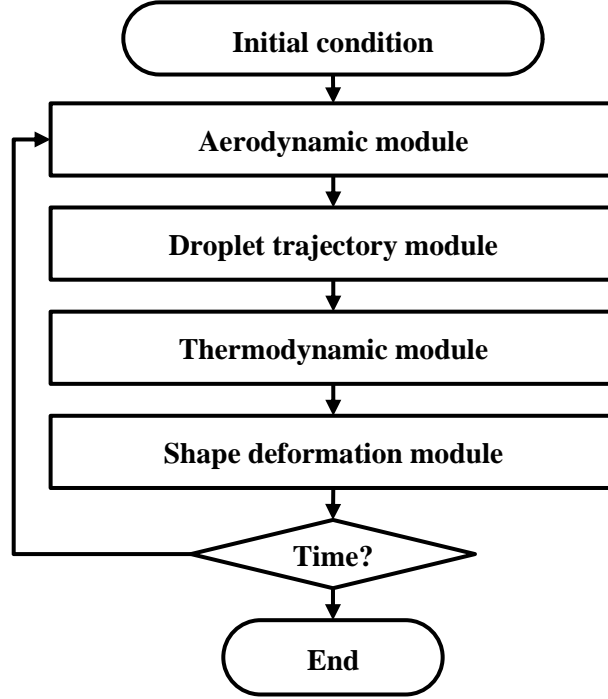


**Figure 1. Modules of the aircraft icing code**

## 2.1 Surface Roughness Model

At the initial stage of icing, water droplets in the air are attached to the aircraft surface in the form of stationary beads after impact. As icing proceeds, the water beads coalesce to grow, and beads over a certain size begin to move in rivulet or film. Thus, surface roughness varies with time, but since the present code assumes a quasi-steady state, numerical modeling of the transient state is limited. Therefore, the current model computes the roughness height for each time-step and calculates the final shape by reflecting the effect of the roughness through interaction with the thermodynamic module. To calculate the surface roughness height, the current model divides the surface state into bead, rivulet, and film state. The surface roughness model consists of four steps as follows.

- (1) The  $h_{\text{bead}}$  and  $h_{\text{film}}$  are calculated by the surface condition according to the icing time.
- (2) Calculate the force equation for the bead state. If the external force of the force equation is smaller than the surface tension, it is assumed to be a bead state.
- (3) Based on the force equation for the water film, it is divided into rivulet and water film states.
- (4) For the next time step, the convective heat transfer coefficient is calculated by reflecting the surface roughness value to the turbulence model.

The model is linked with the thermodynamic module, and determines the water film thickness and the surface roughness according to the surface condition. The surface roughness value was applied to the turbulence model of the aerodynamic module to reflect the effect of model application.

### 2.1.1 Roughness height calculation

The surface roughness height for each surface state with time is calculated according to the geometrical assumption. The surface roughness value of each state is derived from the mass conservation equation of the thermodynamic model of Eq. (1).

$$\rho_w \left\{ \frac{\partial h_f}{\partial t} + \nabla \cdot (h_f U_f) \right\} = \dot{m}_{\text{imp}} - \dot{m}_{\text{ice}} \quad (1)$$

The convection term is split into the incoming and outgoing water film flow mass of the control volume, then the above equation can be expressed as following Eq. (2).

$$\rho_w \frac{\partial h_f}{\partial t} = \dot{m}_{imp} + \dot{m}_{in} - \dot{m}_{ice} - \dot{m}_{out} \quad (2)$$

At the bead state, the  $\dot{m}_{out}$  term can be expressed as 0 because there is no water flow out, and thus the surface roughness in the water droplet state can be expressed by the following Eq. (3). In this case,  $f_{shape}$  is a shape variable, assuming that the shape of the water drop is spherical.

$$h_b = \frac{1}{f_{shape}} \frac{1}{\rho_w} (\dot{m}_{imp} + \dot{m}_{in} - \dot{m}_{ice} - \dot{m}_{out}) \Delta T \quad (3)$$

$$f_{shape} = \sqrt{\frac{\theta_c - \sin \theta_c \cos \theta_c}{2 \sin \theta_c}} \quad (4)$$

For the water film, the water on the surface is flowed by the shear stress of the air force, so the  $\dot{m}_{out}$  can be expressed as in Eq. (5).[8] The equation can be rearranged by substituting the Eq. (1) into the form of the first order ordinary differential equation as shown in Eq. (6).

$$\dot{m}_{out} = \frac{\bar{\tau}}{2\mu_w} h_f^2 \quad (5)$$

$$\rho_w \left\{ \frac{\partial h_f}{\partial t} + \frac{\bar{\tau}}{2\mu_w} h_f^2 \right\} = \dot{m}_{com} + \dot{m}_{in} - \dot{m}_{ice} - \dot{m}_{eva} = \dot{m} \quad (6)$$

The height of the water film height is derived by solving Eq. (6). The height of the water droplet and the water film are used as parameters to calculate the force equilibrium equation of the surface, and calculate the surface condition and the surface roughness height based on this.

### 2.1.2 Force equilibrium equation for surface

The beads on the surface are assumed to be subjected to gravitational and aerodynamic forces acting as the external force, with the surface tension acting as the as reacting force. When the external force is placed on the left side and the surface tension is put on the right side, the following Eq (7) is obtained. At bead state, the surface tension force equilibrates with external force. When the external force exceeds the surface tension, bead flows as rivulet or a water film.

$$\int_0^\pi \sigma_w \cos(\theta(\varphi)) \cos(\varphi) r_b d\varphi = \rho_b g V_b + \tau_w A_b + \int \frac{dp}{dx_i} dV \quad (7)$$

The separation of the water film into rivulet is determined by the magnitude of the force acting on the water film. Gravity, flow shear stress, and pressure act as external forces, as well as water droplets. As in the previous Eq. (7), the force equation for the water film appears as (8). When the external force acting on the water film acts less than the surface tension, only a part of the water film flows, and thus, it changes into a rivulet. Based on Eq. (8), surface state is classified into water film and rivulet.

$$\sigma_w (1 - \cos \theta_c) = \frac{1}{2} \rho_w \left\{ \frac{\tau_w}{\mu_w} y - \frac{y^2}{\mu_w} \left( \frac{dp}{dx} + \rho g \right) \right\}^2 \quad (8)$$

### 2.1.3 Effect of the turbulence model

In this study, a model considering the variation of surface roughness with time was applied to the RANS based aircraft icing code. Surface roughness transition due to ice accretion induces the changes of viscous effect associated relative motion between the fluid and the surface. As the RANS equation focuses on the mean flow properties, application of adequate turbulence model considering the effect of roughness is required. In the case of a general turbulence model, since the analysis is performed on a smooth surface, the convective heat transfer coefficient of the surface is computed small, declining the accuracy of ice shape prediction. Therefore, Spalart-Allmaras model with roughness correction is used [10]. Since the model uses the direct distance information of the surface and the flow field, the surface roughness value can be directly included in the flow field as Eq. (9), where  $d_{new}(s)$  is modified wall distance and  $k_s(s)$  is roughness height.

$$d_{new}(s) = d_{wall} + 0.03k_s(s) \quad (9)$$

The surface roughness increases the size of the turbulent viscosity. Turbulent viscosity is calculated using  $\tilde{\nu}$  obtained by solving Spalart-allamras model[10] using the surface roughness values. This affects the thermal conductivity as shown in Eq. (10).

$$k_{eff} = \rho c_p \left( \frac{\nu}{Pr} + \frac{\nu_{turb}}{Pr_{turb}} \right) \quad (10)$$

The convective heat transfer coefficient, which is an important parameter of icing shape determination, is calculated from the thermal conductivity and the temperature gradient calculated in the aerodynamic module. Since the amount of icing is determined by the heat exchange at the surface, the increase in the convective heat transfer coefficient with increasing turbulent thermal conductivity affects the accuracy of the analysis.

$$h_{cv} = -k_{eff} \frac{\partial T}{\partial n} \left( \frac{1}{T_{sur} - T_{\infty}} \right) \quad (11)$$

### 3 Result and Discussion

In this section, the ice accretion shapes of the simulation with current surface roughness model applied are compared with those of empirical correlation and experiments. First, the validity of the model was evaluated through comparison with the measured roughness height and predicted value of empirical correlation. Then, the runback water mass and heat convection coefficient, which are physical parameters of the model application, are compared with those of empirical correlation. The ice accretion shapes were presented to show the improvement of the model. The test model is two-dimensional NACA0012 and the chord length is 0.5334m. The number of grids is about 57,000, and the mesh is C-type grid as shown in Fig. 2.

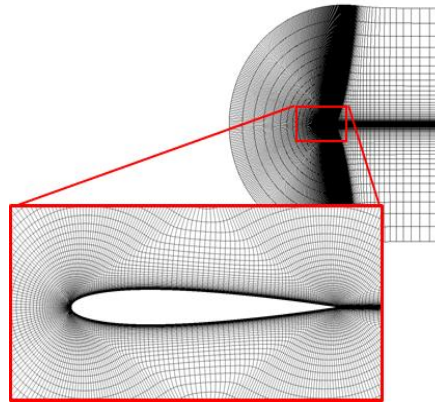


Figure 2. NACA 0012 airfoil grid

### 3.1 Roughness height validation

**Table 1. Cases for surface roughness comparison [2]**

		Conditions		
Airfoil	NACA 0012			
Angle of attack(°)	0			
Airspeed(m/s)	67.1	89.5	111.8	
Temperature(°C)	-1.1	-2.2	-3.9	
LWC(g/m <sup>3</sup> )	0.5	0.75	1.0	1.2

Fig. 3 ~ 5 compare the measured roughness height from Shin [2], and the values obtained by applying the current model and the empirical correlation of NASA[5], according to the change of airspeed, temperature LWC. The conditions are shown in Table 1, and the velocity 67.1m/s, temperature -2.2°C and LWC 0.5g/m<sup>3</sup> case was the basis for each analysis.

The results of the experiment and the present model were measured at 5 ~ 10 mm from the leading edge of the top surface where the rough region appeared. For the empirical correlation, the result calculated according to the equation in Ref. 5 is used. When the present model is applied, there is a similar trend for LWC and temperature, but there is no significant correlation for airspeed.

According to Fig. 3, the experimental data are not affected by the airspeed, while, the empirical correlation results increase linearly. In the present model, the shear stress due to aerodynamics is large, and thus the surface roughness of the water droplets formed is gradually decreasing. In case of LWC, experimental value and current model show similar values to experimental measurements. Empirical correlations tend to increase as well, however the rate is much greater. This is because the equation was approximated by a quadratic relation of LWC [5]. For the temperature, the empirical correlation results are large for the experimental data and the present model, but it was found to increase linearly.

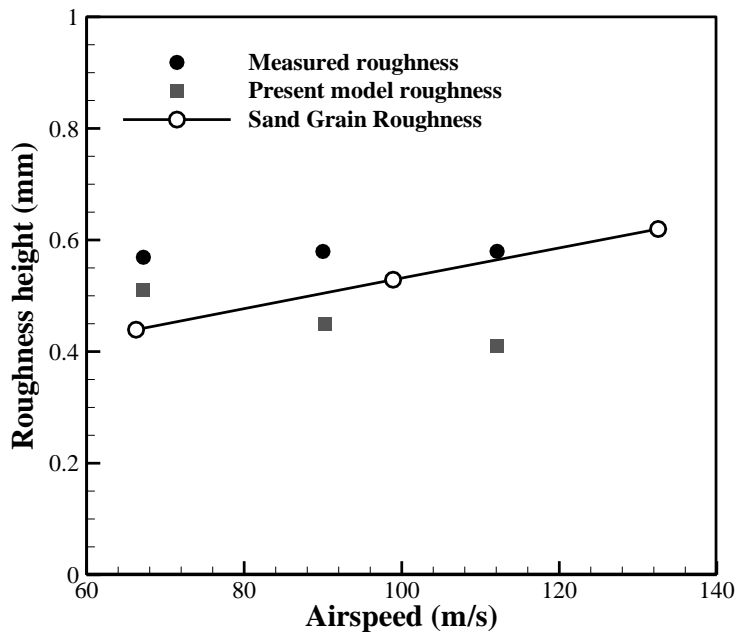


**Figure 3 Roughness height due to airspeed**

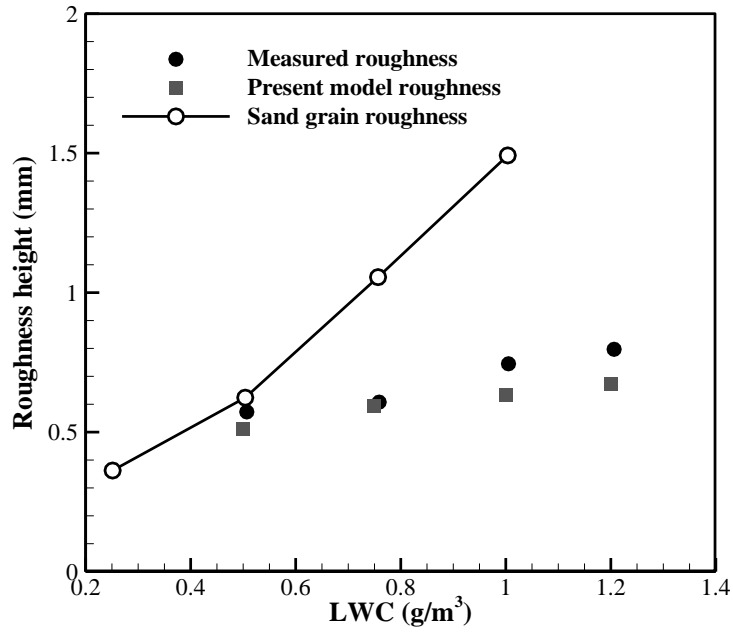


Figure 4 Roughness height due to LWC

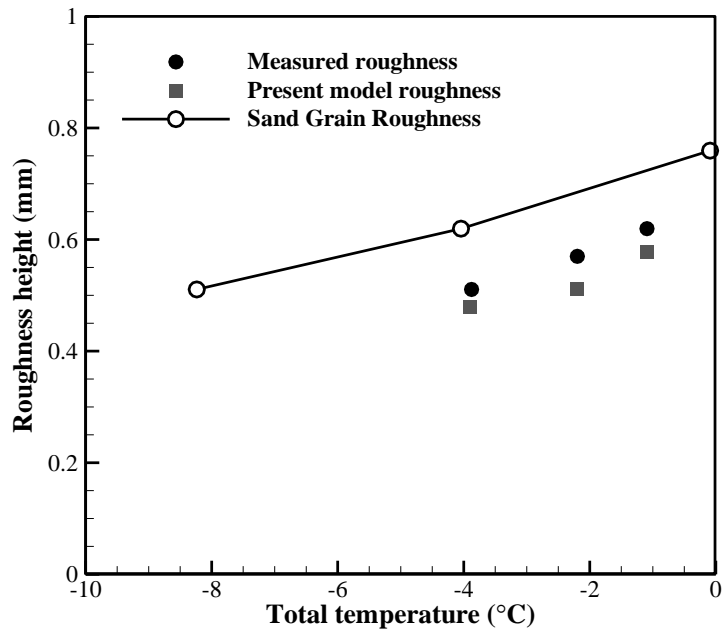


Figure 5 Roughness height due to temperature

For the current model, the roughness height is expressed as a distribution type. Fig. 6 shows the roughness height distribution according to the change of LWC. The roughness height increases rapidly from the leading edge to the trailing edge. As presented in Fig. 5, the maximum roughness height is predicted between 5 and 10 mm at the leading edge. The distribution of these models more closely aligns experimental values and trends while empirical correlation provides a single value.

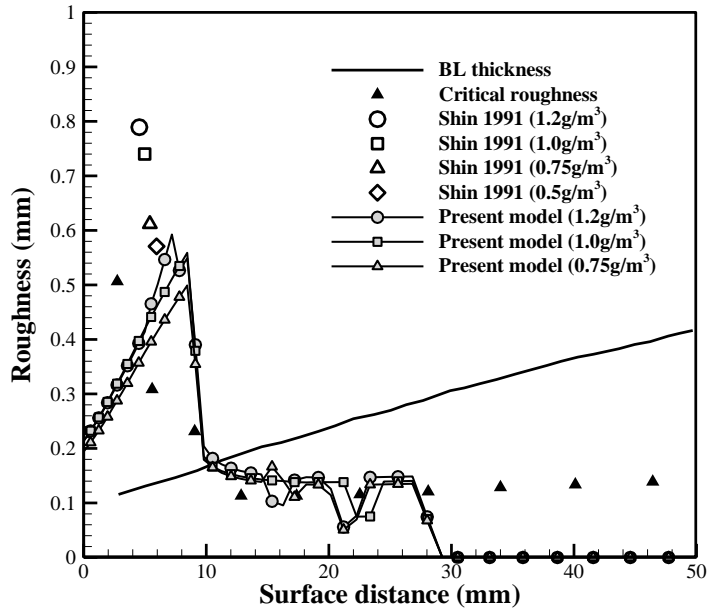


Figure 6 Roughness height distribution for LWC change

### 3.2 Effect due to surface roughness model

The current model was evaluated through numerical simulation for 4 different conditions presented in Table 2. The values of runback water mass and heat convection coefficient were compared with the empirical correlation results to see the change of parameters according to the application of surface roughness model. Then the current model was evaluated by comparing the ice accretion shape of the experiment and numerical simulations with two different model.

Table 2. Ambient conditions to validate the current model [12]

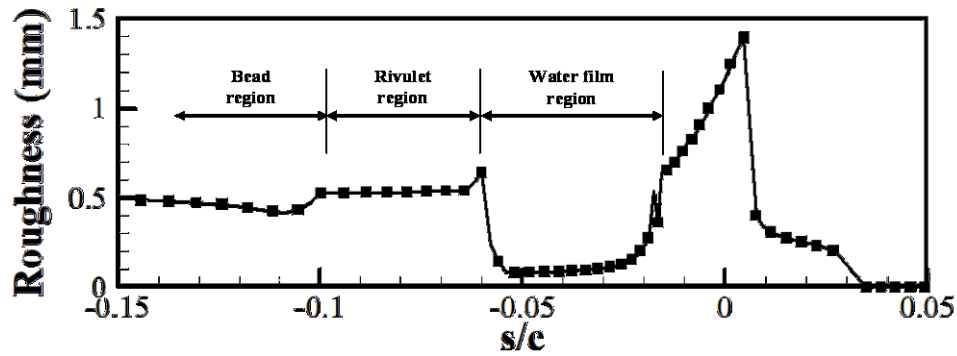
	Case 1	Case 2	Case 3	Case 4
Chord (m)	0.5334			
Angle of attack(°)	4			
Airspeed(m/s)	102.8	67.1	102.8	67.05
Temperature(°C)	-9.71	-8.06	-11.15	-28.3
LWC(g/m <sup>3</sup> )	0.55	1.0	1.3	1.0
MVD(μm)	20	20	20	20
Time(s)	420	360	360	360

#### 3.2.1 Runback water

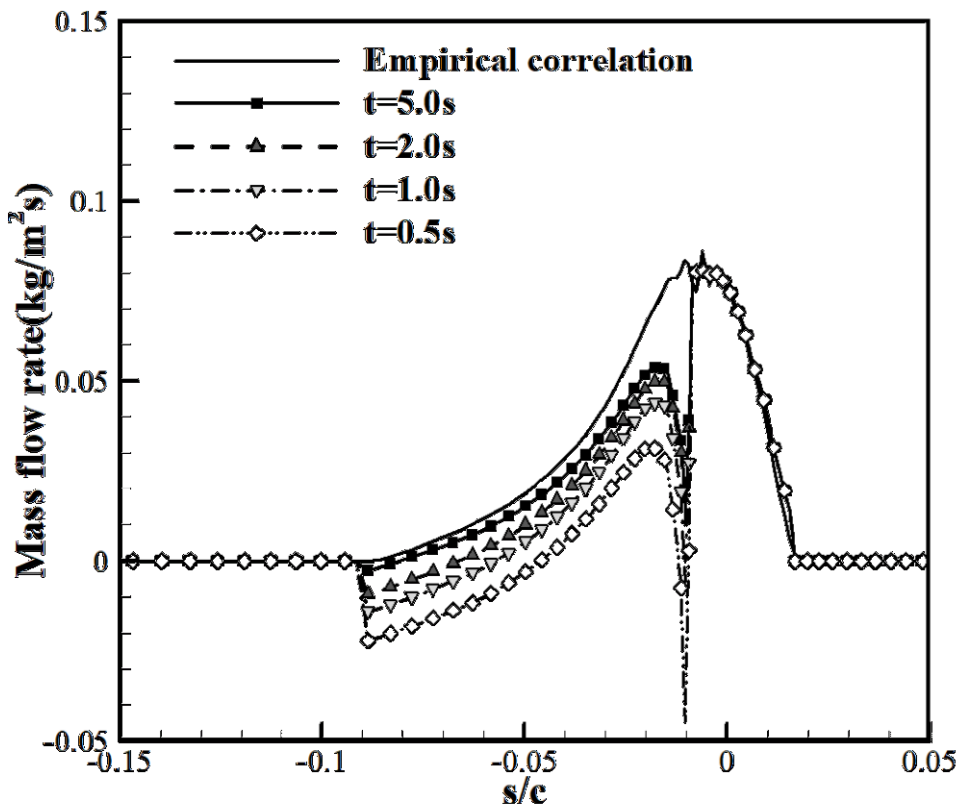
Fig 7 presents the roughness height and runback water mass according to ice accretion time for case C. As shown in Fig. 7 (a), the present roughness model computes the local roughness height depending on the region. Near the stagnation point, where the collection efficiency is high, and a water film is formed owing to the high-impinging water mass. In this smooth zone, a low roughness height is predicted. In contrast, on moving to the trailing edge, the remaining water mass decreases, and the rivulet and bead appear to exhibit a large roughness height.

Fig. 7 (b) compares the time-dependent change of the runback water flow rate with the model application and the result of empirical correlation application. For the first 2 seconds, the runback mass

is negative in the rivulet region on the bottom. This is because initially small rivulets are formed and flow more than the amount of water leaving the control volume. Thereafter, the area of the water film increases near the stagnation point and the runback mass increases as the size of the rivulet increases. As the current model is applied, the surface state is divided into three regions of water film, rivulet, and bead, and it is confirmed that the runback mass is affected accordingly.



(a) Roughness distribution



(b) Water runback mass

Figure 7 Roughness distribution and water runback mass for case C

### 3.2.2 Heat convection coefficient

The present roughness model computes the local roughness height from the surface, as shown in Fig 8. Near the stagnation point, the collection efficiency is high, and a water film is formed owing to the high-impinging water mass. In this smooth zone, a low roughness height is predicted. In contrast, on moving to the trailing edge, the remaining water mass decreases, and the rivulet and bead appear to exhibit a large roughness height. Particularly on the upper surface, the bead height is greater owing to the aerodynamic force with a strong favorable pressure gradient.

Fig 9 displays the heat convection coefficient difference when applying the roughness models. In contrast with the difference in the roughness height in the smooth zone, the heat convection coefficient difference is about 20% and there is no significant difference in the ice shape. Currently, the effect of surface roughness is shown only by the enhancement of the thermal conductivity with the present aircraft icing code. Near the ice horn region, where larger roughness value is predicted, heat convection coefficient also increased, affecting the shape of the ice afterwards.

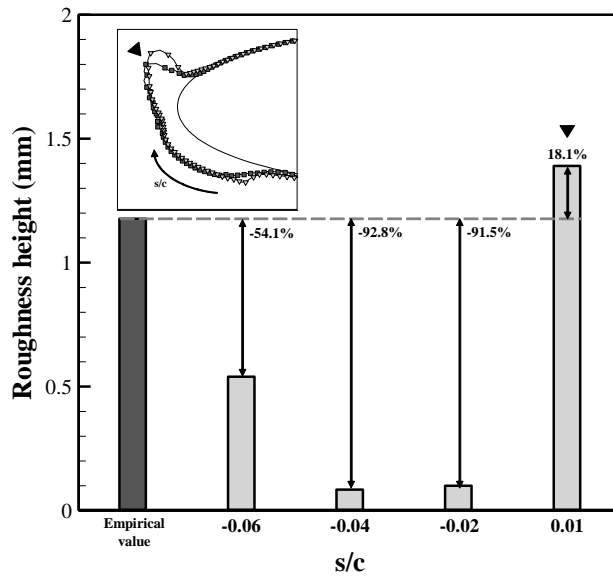


Figure 8 Roughness comparison for case C

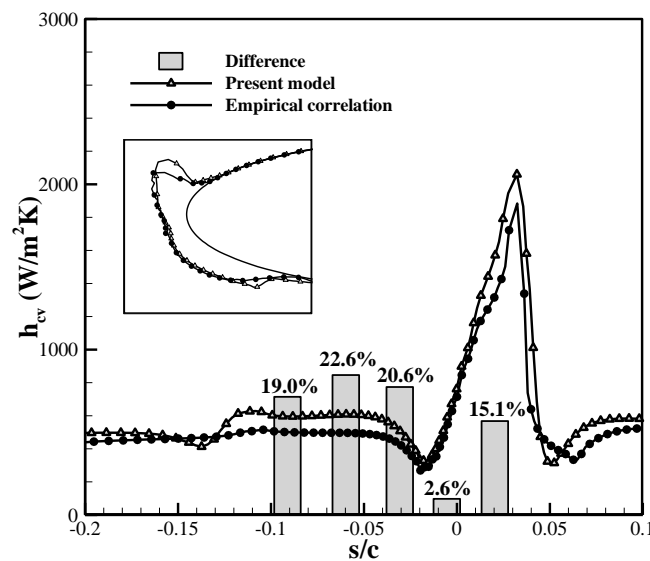


Figure 9 Heat convection coefficient for case C

### 3.3 Ice shape comparison

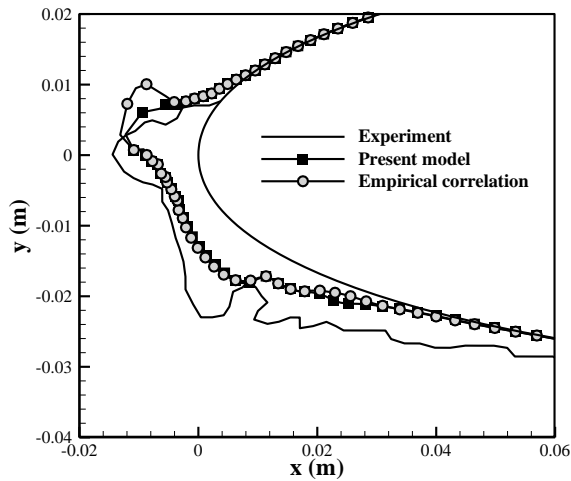


Figure 10 Ice shape for case A

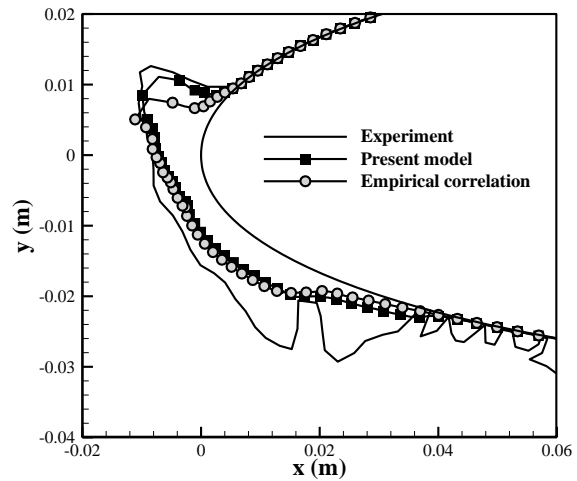


Figure 11 Ice shape for case B

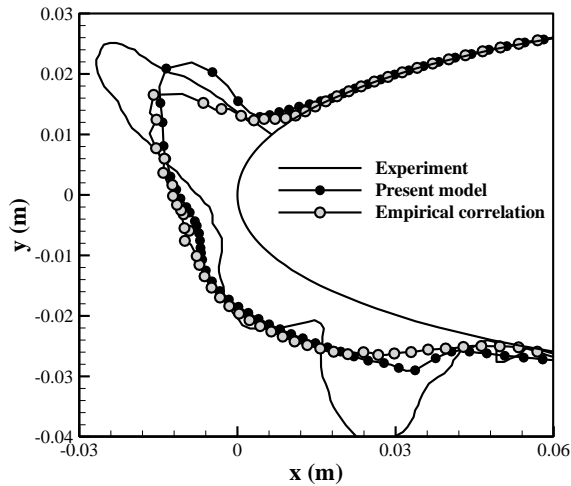


Figure 12 Ice shape for case C

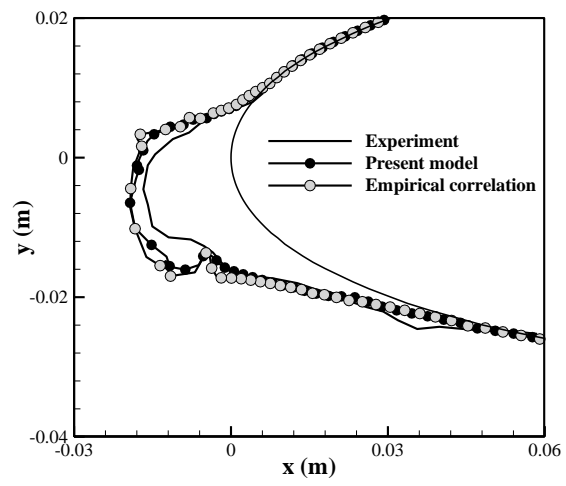
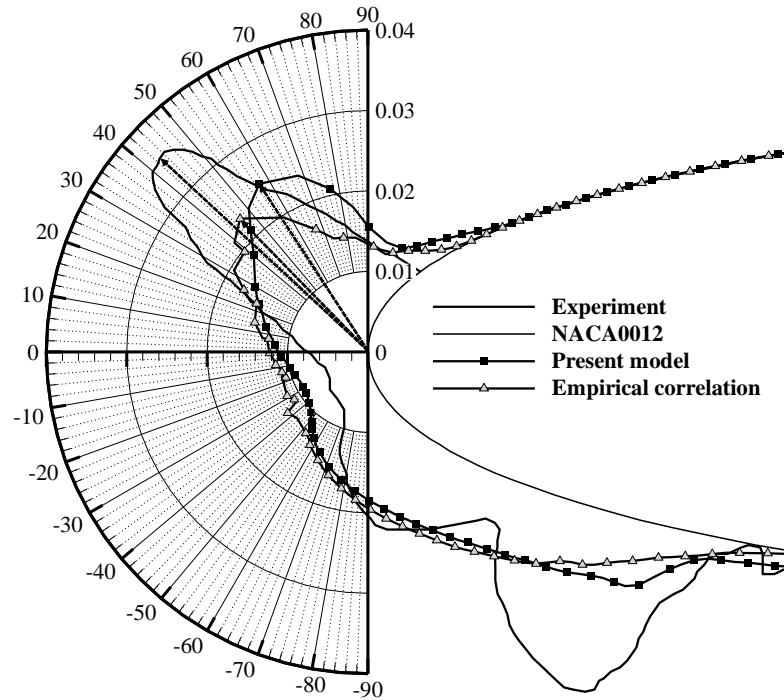


Figure 13 Ice shape for case D

The final ice shapes for both roughness models are depicted in Fig. 10 ~ 13 for mixed ice case where glaze and rime ice appears together. For the mixed ice case, the overall ice accretion shapes from both models are similar but the present model predicts the size of ice horn on the upper surface similar to the experimental values. Ice horn is important for the aerodynamic characteristic of iced airfoil.

In Fig. 10, case A, the result from the present model predicts ice horn similar in size to the experimental values on the upper surface, which predicts a smaller ice horn than those of empirical correlation. For this case, the roughness element is formed small due to low LWC. The reduction of the roughness height is also related to the size of the heat convection coefficient, which is the most dominant factor in the energy equation for determining the thickness of ice. This leads to a contraction of ice accretion rate.

Case B and case C is humid condition with LWC over than  $1.0\text{g/m}^3$ . Under this condition, the present model shows the large ice horn shapes. Since, local roughness height is distinguished by the present model, near stagnation point, smooth zone appears owing to water film and computes higher roughness value for rough region near ice horn. Therefore, the ice thickness near the rough region shows an improved result, but in the direction of the ice growth, the current model appears to be shifted backward. As shown in Fig. 14, case C, the ice horn is expected to grow about 57 degrees from the leading edge when the present model applied, but the experiment value is about 44 degrees.



**Figure 14 Ice horn growth for case C**

When surface roughness is generated, ice tends to grow in the direction in which droplets fly because water droplets hit the roughness element and freeze. The present study does not discuss the ice formation direction due to surface roughness. Therefore when calculating the shape of the current ice, we move the mesh perpendicular to the surface by the ice thickness predicted from each control volume.

Fig 13 presents the ice shape for the low temperature case where rime ice dominantly appears. In contrast with case A ~ C, all the results exhibit a similar ice shape. In the rime case, most droplets freeze owing to the low temperature and there is a slight runback water flow. Therefore, for the rime case, the shape difference is ignorable for different roughness model.

In summary, because the empirical correlation predicts the roughness height by extrapolating the existing results, it predicts a much higher roughness height and heat convection coefficient, resulting in concentrated ice accretion locally. The roughness height is partly calculated when the current model is applied, and the ice shape indicates an improved feature. However, for all the cases, the numerical results underestimate the ice shape, particularly for a lower surface. The thermodynamic model currently used in the numerical simulations predicts ice shapes from a macroscopic point of view based on the mass conservation and energy conservation relations with a control volume. However, according to a previous observation regarding the ice accretion process, the roughness element is responsible not only for the heat convection enhancement, but also for the microscopic motion, which the current numerical method does not model, such as the increase in the local collection efficiency. Therefore, a study on simulating the effect of surface roughness is required.

## 4 Conclusion

This study proposes an improved surface roughness model for application in an aircraft icing code based on the Navier–Stokes equation. The concept of the model was to distinguish three surface states based on the film thickness and to compute the roughness height. For the implementation of the model with a quasi-steady state solver, a new analytical model derived from the governing equation of the thermodynamic module was introduced. The proposed methodology was verified by other roughness models. The findings of the study are as follows:

1) This study extended the physical roughness model to Aircraft icing code based on Navier - Stokes equations to consider the inherently unsteady characteristics of surface roughness. Since the aircraft

icing solver assumes the quasi-steady assumption for numerical efficiency, the present model predicts the surface roughness by using analytical model derived from governing equation of the thermodynamic module of aircraft icing solver. Through this procedure, the transient roughness height can be obtained by simply applying the model to current Navier-stokes based aircraft icing solver. Also, by interacting with the turbulent model of Aerodynamic module, the effect of roughness modification was reflected through the heat convection coefficient affecting the ice accretion shape.

2) Compared with the conventional empirical correlation, it was confirmed that the shape is better predicted for some conditions. The correlation results excessively predicted the surface roughness value especially under the high LWC conditions, and the ice accretion mass was predicted high in the smooth region. On the other hand, as a result of application of the current model, the surface roughness value is calculated similar to the measured value in the experiment, and the shape tendency is improved.

Along with the advances in the methodology, this study showed the limitations of the existing models, and in some cases, it predicted an improvement in the ice shape. It was confirmed that the physical model for the roughness height was reliable, and the empirical parameters were eliminated to be applied to the Navier–Stokes solver-based aircraft icing code. However, there were some limitations of implementing this model alone to the icing code to predict the surface roughness. Because the effect of surface roughness was not fully considered, except for the heat convection enhancement, further investigation is required for accurate calculations. Nevertheless, this study has laid the basis for a heuristic approach for a more advanced modeling based on physical phenomena.

## 5 Acknowledgement

This work was supported by the Korea Agency for Infrastructure Technology Advancement(KAIA) grant funded by the Ministry of Land, Infrastructure and Transport (Grant 18CHTR-C128889-02)

## References

- [1] R. J. Hansman, and S. R. Turnock, Investigation of Surface Water Behavior During Glaze Ice Accretion, *J. Aircraft* 25. 2: 140-147, 1989
- [2] J. Shin, Characteristics of Surface Roughness Associated with Leading Edge Ice Accretion, NASA TM-106459, 1994
- [3] D. N. Anderson, and J. Shin, Characterization of Ice Roughness from Simulated Icing Encounters, NASA TM 107400, 1997
- [4] R. Gent, R. Markiewicz, and J. Cansdale, “Further studies of helicopter rotor ice accretion and protection,” *Vertica* 11: 473-492. 1987
- [5] G. A. Ruff, and B. M. Berkowitz, Users’ Manual for the NASA Lewis Ice-Accretion Prediction Code (LEWICE), NASA CR 185129, 1990
- [6] G. Fortin, A. Ilinca, J.-L. Laforte, and V. Brandi, New roughness computation method and geometric accretion model for airfoil icing, *J. Aircraft* 41. 1:119-127, 2004
- [7] G. Croce et al., FENSAP-ICE: Analytical model for spatial and temporal evolution of in-flight icing roughness, *J. Aircraft* 47. 4: 1283-1289, 2010
- [8] H. Beaugendre et al., FENSAP-ICE’s three-dimensional inflight ice accretion module: ICE3D, *J. of Aircraft* 40.2: 239-247, 2003
- [9] OpenFOAM, Open-source Field Operation and Manipulation, Software Package, Ver. 2.2.0, 2011, <http://www.openfoam.com>
- [10] B. Aupoix and P. R. Spalart. Extensions of the Spalart–Allmaras turbulence model to account for wall roughness, *Int. J. Heat and Fluid Flow* 24. 4:454-462, 2003
- [11] C. Son, S. Oh, and K. Yee, Ice accretion on helicopter fuselage considering rotor-wake effects, *J. Aircraft* 54. 2:500-518, 2016
- [12] Wright, W. B., Rutkowski, A., Validation Results for LEWICE 2.0, NASA/CR-1999-208690, 1999